Supplementary Information to accompany

Tug-of-war of microtubule filaments at the boundary of a kinesin- and dynein-patterned surface

Junya Ikuta, Nagendra K. Kamisetty, Hirofumi Shintaku, Hidetoshi Kotera, Takahide Kon and Ryuji Yokokawa

*Ryuji Yokokawa

Department of Micro Engineering

Kyoto University

C3-c2S18, Kyoto-daigaku Katsura, Nishikyo, Kyoto

615-8540 JAPAN

Tel/FAX: +81-75-383-3682

Email: ryuji@me.kyoto-u.ac.jp

Contents

1 Supplementary Figures 3
2 Supplementary Table 7
3 Supplementary Discussion 8
4 Supplementary Methods 11
4.1 Measurement of $<d_k>$ and $<d_d>$ 11
4.2 Functions for N_d/N_k– and N_k/N_d–velocity curves 12
5 Supplementary Video 15
6 Supplementary References 16

1 Supplementary Figures

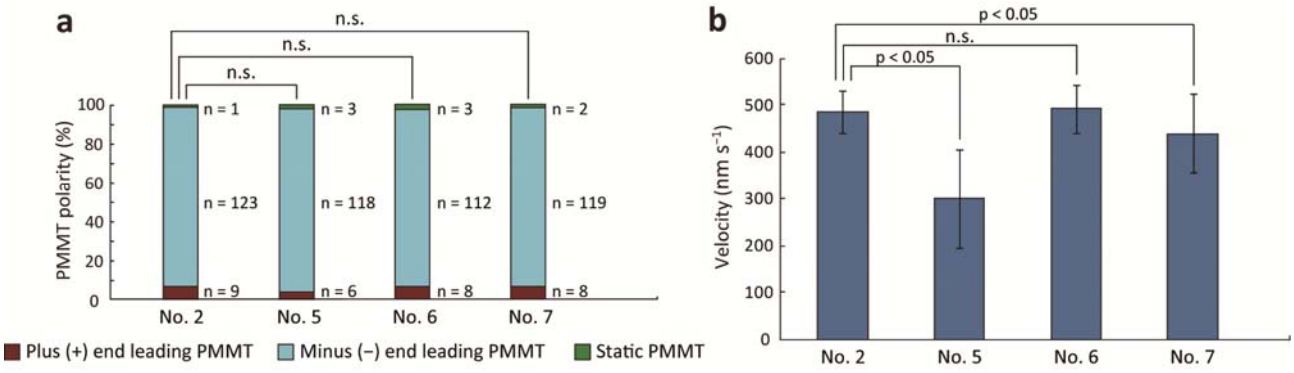

Fig. S1. (**a**) Polarity and (**b**) velocity of PMMTs gliding on the glass region prepared by assay sequences No. 2, 5, 6, and 7 in Table S1. (n = 100 for each assay in **b**, error bars represent s.d.) n.s. = not significant.

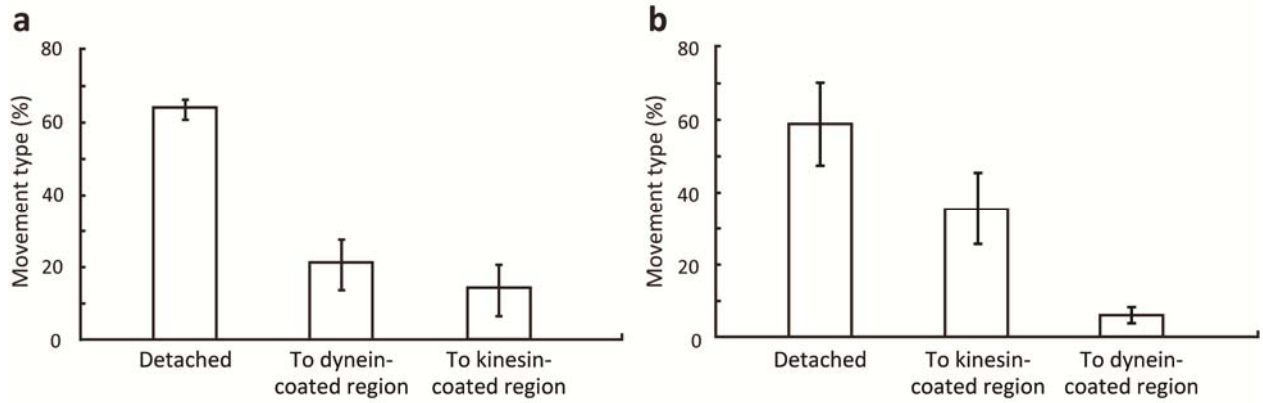

Fig. S2. Behaviour of MTs approaching from (**a**) the dynein-coated region to the boundary (group 1) and (**b**) the kinesin-coated region to the boundary (group 2). In group 1, of the observed MTs (n = 286), 64.3 ± 2.8% (mean ± s.d.) were detached from the surface, 21.3 ± 7.1% returned to the original dynein-coated region, and 14.3 ± 7.0% passed the boundary and continued gliding in the kinesin-coated region. In group 2, of the observed MTs (n = 168), 58.9 ± 11.3% (mean ± s.d.) were detached from the surface, 35.1 ± 10.3% returned to the original kinesin-coated region, and 6.0 ± 1.4% passed the boundary and continued gliding in the dynein-coated region.

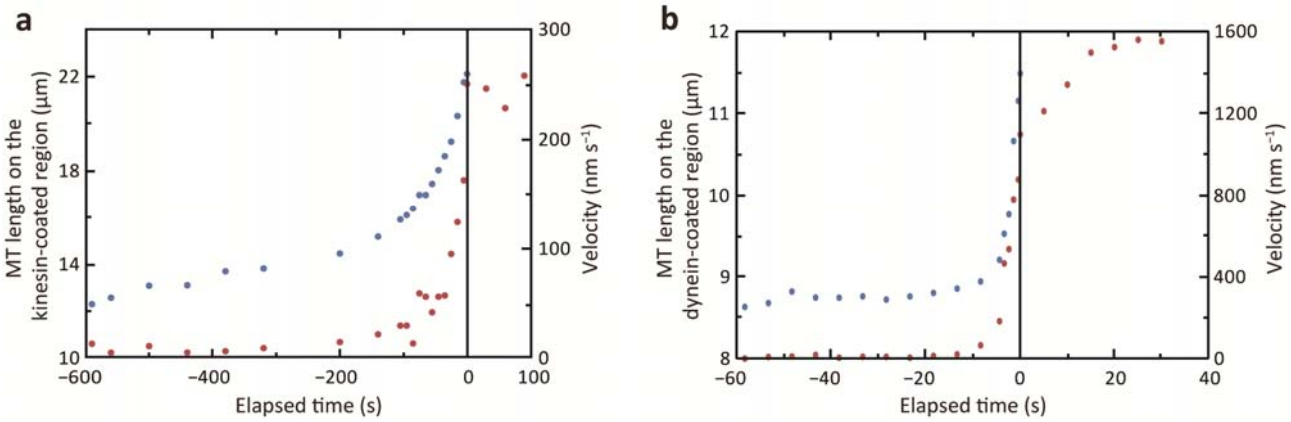

Fig. S3. A set of MT length (blue plots) and velocity (red plots) without normalization during tug-of-war for MTs gliding to (*a*) the kinesin-coated region and (*b*) the dynein-coated region.

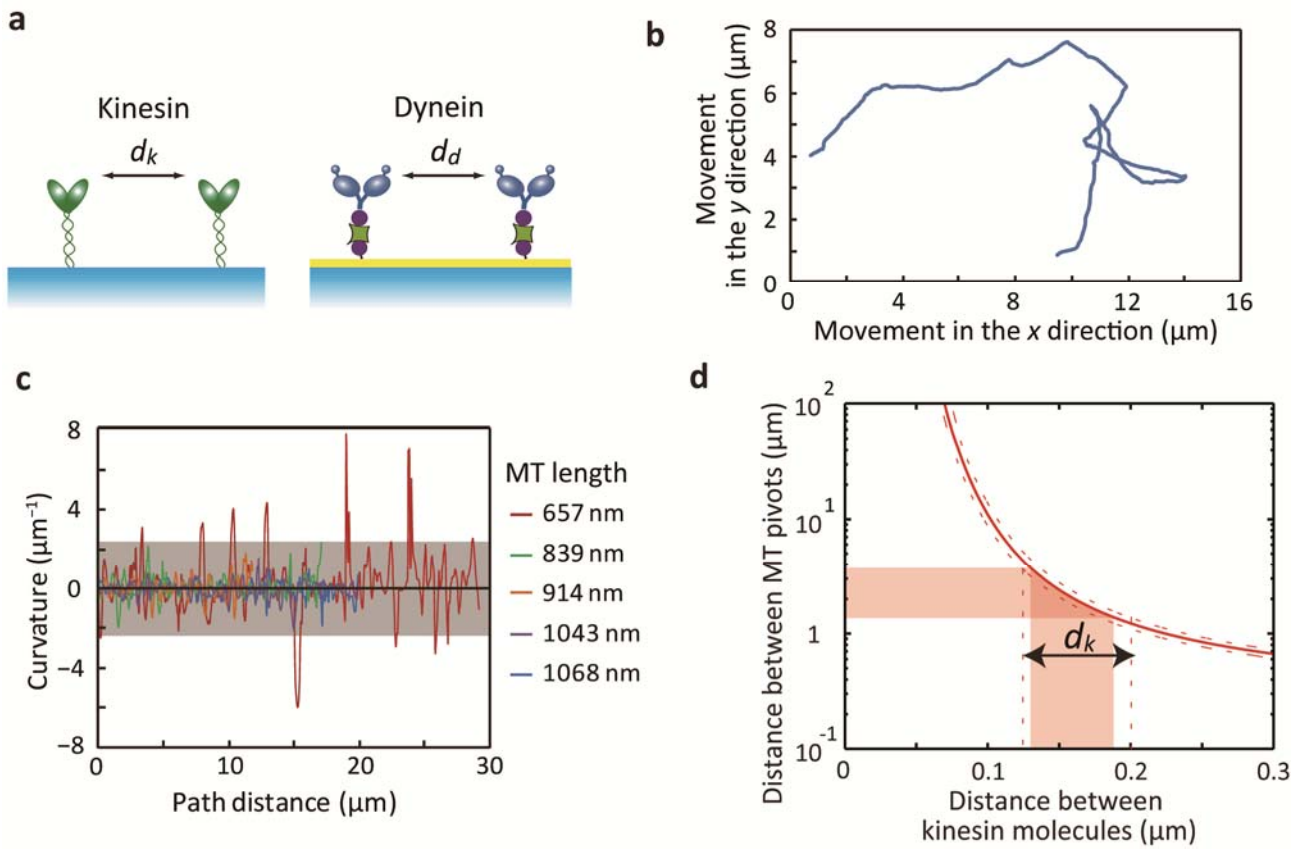

Fig. S4. Measurement of <d_k> and <d_d>. (*a*) Schematic of <d_k> and <d_d>. (*b*) Trajectory of a MT with acute pivoting in the kinesin-coated region. (*c*) Curvatures of five MTs: the red plot was obtained from the trajectory shown in (*b*), and the other four are from longer MTs. (*d*) The relationship between <*S*> and <d_k>. Margins are indicated by the dashed lines to determine <d_k>.

2 Supplementary Table

Table S1. Sequence of protein coating used for optimizing selective kinesin and dynein patterning.

Assay No.	Injection sequence				Gold with SAM region	Glass region
	1	2	3	4		
1	K	−	−	−	MT gliding by kinesin	MT gliding by kinesin
2	P	K	−	−	MT gliding by kinesin; weak MT binding to the surface	MT gliding by kinesin
3	SA	D	−	−	MT gliding by dynein	MT gliding by dynein
4	P	SA	D	−	MT gliding by dynein	No MT attachment
5	P	K	SA	D	MT gliding by dynein	MT gliding by kinesin
6	P	K	SA	−	NA	MT gliding by kinesin
7	P	K	D	−	NA	MT gliding by kinesin

K, kinesin, D, dynein, P, Pluronic F108, SA, streptavidin, NA, not applicable.

3 Supplementary Discussion

Optimization of the protein coating sequence. To determine the optimum protein coating sequence for the selective coating of dynein on the SAM-coated gold region and kinesin on the bare glass region, we examined binding of motors and the blocking reagent Pluronic F108 to each surface. After microfabrication and SAM formation as described in Methods in the main text, we varied the injection sequence of the kinesin (abbreviated as K in Table S1), dynein (D), Pluronic F108 (P), and streptavidin (SA) solutions, all of which were prepared as used for selective kinesin and dynein patterning in Methods. Protein-coated regions were evaluated by examining the polarity and velocity of PMMTs, and the assay conditions were the same as those described in Methods. The injection sequence and qualitative results are summarized in Table S1.

Purified kinesin can be non-specifically immobilized on bare or Pluronic-coated glass surfaces[1]. Assay No. 1 indicated that kinesin non-specifically bound not only to the glass surface but also to the SAM surface. To block this non-specific binding, we introduced Pluronic in assay No. 2. Although the number of MTs gliding on the SAM surface was decreased, some MTs were found gliding in the SAM-coated region. In assay No. 3, we confirmed MT gliding supported by dynein immobilized on the SAM with streptavidin in between. However, at this stage we found that MTs in the glass region were also gliding by dynein, which was immobilized through streptavidin or nonspecific dynein binding to the glass surface. Because we know that Pluronic can prevent binding of streptavidin and dynein to the glass surface in a separate assay, Pluronic was first incubated before streptavidin and dynein coating in assay No. 4. This procedure successfully

limited dynein binding only to the SAM-coated region, because no MTs were captured in the glass region. According to the manufacturer's specifications, casein may contain biotin and cause interference with the streptavidin-biotin bindings. However, as we introduced the streptavidin solution with 0.5 mg ml^{-1} casein as described above, this contamination does not affect our selective motor coating. It is also confirmed in a reported assay[2].

The last step was to incorporate kinesin into the sequence while retaining the selective binding of dynein. We expected that assay No. 5 would contain the optimum sequence based on two facts: (i) Pluronic reduces nonspecific binding of kinesin to SAM (assay No. 2), and (ii) kinesin injection over a dynein-coated surface results in a mixture of the two motors. Two regions prepared using the assay No. 5 sequence were evaluated by determining the polarity and velocity of gliding PMMTs; selective kinesin and dynein coating was successful as discussed in the main text.

We further conducted two experiments to understand why the velocity was reduced in the glass region in assay No. 5. Because the possible causes were streptavidin or dynein coating after kinesin incubation, we examined each effect on MT gliding in assays No. 6 and No. 7. The results for polarity and velocity are summarized in Fig. S1a and b, respectively, along with results for the control experiment and assay No. 5. Although streptavidin or dynein injection over the kinesin-coated glass surface did not affect PMMT polarity (Fig. S1a), dynein lowered the velocity (Fig. S1b). The velocity difference between assay No. 5 and No. 7 might be caused by the total amount of nonspecifically immobilized dynein due to the existence of streptavidin. Therefore, as discussed in the main text, dynein may act as a physical "roadblock" to MT gliding because of its size. Even

with this velocity decrease, we concluded that assay No. 5 is the optimum order for selective kinesin and dynein coating.

4 Supplementary Methods

4.1 Measurement of $\langle d_k \rangle$ and $\langle d_d \rangle$

A theoretical model was reported based on the stochastic evolution of the number of motors bound to the filament[3], for which the average distance travelled between acute pivoting of a short MT, $\langle S \rangle$, is given by

$$\langle S \rangle = \frac{L + 2\langle d \rangle}{L + 3\langle d \rangle} \frac{\langle d \rangle^2}{L} \left(e^{\frac{L}{\langle d \rangle}} - 1 - \frac{L}{\langle d \rangle} \right) \quad \text{(S1)}$$

where L is the MT length and $\langle d \rangle$ is the average tip length. Based on equation (S1) with experimentally measured values for $\langle S \rangle$ and L, Van den Heuvel *et al*. obtained $\langle d \rangle = 0.10 \pm 0.02$ μm for kinesin immobilized on a fused-silica channel surface[3]. We used this method to obtain the average distance between kinesin molecules, $\langle d_k \rangle$, on the bare glass surface, and between dynein molecules, $\langle d_d \rangle$, on the SAM-coated surface (Fig. S4a).

Kinesin- or dynein-coated regions were prepared by assay sequences No. 2 and No. 4, respectively. MTs were shortened by shearing through a syringe, which produces MTs with an average length of 1.05 ± 0.54 μm. They were introduced to the flow cell, and L and $\langle S \rangle$ for the kinesin-coated region were measured according to the methods of Van den Heuvel *et al*.[3] as follows: $L = 0.67 \pm 0.03$ μm for 10 different images on the same MT and $\langle S \rangle = 2.5 \pm 1.1$ μm for that MT. Fig. S4b shows the trajectory of that MT for 240 s. Curvatures of the MT and of four other longer MTs are plotted in Fig. S4c. The shortest MT had many pivot points, and their average interval was measured as above. The relationship between $\langle S \rangle$ and $\langle d \rangle$ described in equation (S1) is plotted in Fig. S4d, which enabled us to calculate $\langle d_k \rangle$ as 0.16 ± 0.04 μm. The corresponding values for the

dynein-coated region were measured as $L = 0.52 \pm 0.02$ μm and $\langle S \rangle = 4.0 \pm 2.3$ μm, and the resulting value for $\langle d_d \rangle$ was 0.10 ± 0.02 μm (graphs are not shown).

4.2 Functions for N_d/N_k– and N_k/N_d–velocity curves

Model 1: For MTs gliding to the kinesin-coated region, the conventional force-velocity relationship for a single motor[4],

$$v_{MT} = v_k[1 - (F/f_k)^{w_k}] \quad \text{(S2)}$$

is rewritten as a function of N_d/N_k and w as discussed in the main text by assuming the load force, $F_{Total} = N_d f_d^*$, is shared by N_k kinesins with the stall force, f_k. The function is as follows:

$$v_{MT}/v_k = 1 - (N_d f_d^*/N_k f_k)^{w_k}. \quad \text{(S3)}$$

In the same manner, for MTs gliding to the dynein-coated region,

$$v_{MT} = v_d[1 - (F/f_d)^{w_d}] \quad \text{(S4)}$$

can be rewritten as:

$$v_{MT}/v_d = 1 - (N_k f_k^*/N_d f_d)^{w_d}. \quad \text{(S5)}$$

Equations (S3) and (S5) were fitted (solid lines) to Fig. 3e and Fig. 3f, respectively, using the least-squares method to calculate f_d^*/f_k, w_k, f_k^*/f_d, and w_d as summarized in Table 1.

Model 2: When the backward velocity is taken into consideration[5-7], the MT velocity is expressed using the load that acts on a forward motor, kinesin (F_+), and a backward motor, dynein (F_-). In other words, F_+ and F_- are generated by dynein and kinesin, respectively. MT velocity,

$$v_{MT} = v_k[1 - (F_+/f_k)^{w_k}], \quad \text{(S6)}$$

is defined for kinesin moving in the forward direction. For the same MT, velocity is also expressed using the dynein backward velocity, v_{db}, as follows:

$$v_{MT} = -v_{db}[1 - (F_-/f_d^*)^{w_d}]. \quad \text{(S7)}$$

Based on the assumption that (i) opposing motors work as a load, and (ii) motors share the load, the force balance on the MT that is pulled by N_k plus and N_d minus motors, $N_kF_+ = N_dF_-$, yields the normalized velocity, v_{MT}/v_k. Here, we consider the linear force-velocity relationship, *i.e.*, $w_k = w_d = 1$, in Model 2, which leads to

$$\frac{v_{MT}}{v_k} = \frac{1-(f_d^*/f_k)(N_d/N_k)}{1+(v_k/v_{db})(f_d^*/f_k)(N_d/N_k)}. \quad \text{(S8)}$$

as shown in the main text. When a MT is pulled by dynein, and kinesin works as a load, one can derive the corresponding equations to (S6) and (S7) as

$$v_{MT} = v_d[1 - (F_+/f_d)^{w_d}], \quad \text{(S9)}$$

and

$$v_{MT} = -v_{kb}[1 - (F_-/f_k^*)^{w_k}]. \quad \text{(S10)}$$

Again, the linear force-velocity relationship leads to

$$\frac{v_{MT}}{v_d} = \frac{1-(f_k^*/f_d)(N_k/N_d)}{1+(v_d/v_{kb})(f_k^*/f_d)(N_k/N_d)}. \quad \text{(S11)}$$

Equations (S8) and (S11) are expressed as dashed lines in Fig. 3e and Fig. 3f in the main text to calculate f_d^*/f_k and v_{db} and f_k^*/f_d and v_{kb}, respectively.

Model 3: As the nonlinear force-velocity relationship is also widely accepted in multi-motor transport, we examined the equations used in Model 2 with different linear/nonlinear parameters between kinesin and dynein: $w_k = 2$ and $w_d = 0.5$[8]. This yields an MT velocity of

$$v_{MT} = v_k[1 - (F_+/f_k)^2], \quad \text{(S12)}$$

for forward kinesin motors and

$$v_{MT} = -v_{db}[1 - (F_-/f_d^*)^{0.5}] \quad \text{(S13)}$$

for backward dynein motors, where the MT glides to the kinesin-coated region. In addition to equations (S12) and (S13), force balance on the MT, $N_kF_+ = N_dF_-$, yields the normalized velocity

v_{MT}/v_k, which was solved using Matlab software (MathWorks) for the curve fit to Fig. 3e (dotted lines). Fitting parameters f_d^*/f_k and v_{db} were obtained as shown in Table 1. For the other MTs gliding to the dynein-coated region, the corresponding equations are

$$v_{MT} = v_d[1 - (F_+/f_d)^{0.5}], \quad \text{(S14)}$$

and

$$v_{MT} = -v_{kb}[1 - (F_-/f_k^*)^2]. \quad \text{(S15)}$$

Equations (S14) and (S15) were used to obtain f_k^*/f_d and v_{kb} by curve fitting in Fig. 3f.

5 Supplementary Video

Video S1. PMMTs gliding on the dynein-coated region of a selectively coated substrate (2× real time).

Video S2. PMMTs gliding in the kinesin-coated region of a selectively coated substrate (20 × real time).

Video S3. MT experiencing tug-of-war at the boundary of the dynein-coated (left) and kines in-coated (right) regions and eventually gliding to the kinesin-coated region (20× real time).

6 Supplementary References

1. Fujimoto, K. *et al.* Colocalization of quantum dots by reactive molecules carried by motor proteins on polarized microtubule arrays. *ACS Nano* **7**, 447-455 (2013).

2. Nitzsche, B. *et al.* Chapter 14 - studying kinesin motors by optical 3d-nanometry in gliding motility assays. *Methods Cell Biol.* **95**, 247-271 (2010).

3. Van Den Heuvel, M. G., De Graaff, M. P., Dekker, C. Microtubule curvatures under perpendicular electric forces reveal a low persistence length. *Proc. Natl. Acad. Sci. U SA* **105**, 7941-7946 (2008).

4. Kunwar, A., Mogilner, A. Robust transport by multiple motors with nonlinear force-v elocity relations and stochastic load sharing. *Phys. Biol.* **7**, 16012 (2010).

5. Muller, M. J., Klumpp, S., Lipowsky, R. Tug-of-war as a cooperative mechanism for bidirectional cargo transport by molecular motors. *Proc. Natl. Acad. Sci. USA* **105**, 4 609-4614 (2008).

6. Kunwar, A. *et al.* Mechanical stochastic tug-of-war models cannot explain bidirection al lipid-droplet transport. *Proc. Natl. Acad. Sci. USA* **108**, 18960-18965 (2011).

7. Svoboda, K., Block, S. M. Force and velocity measured for single kinesin molecules. *Cell* **77**, 773-784 (1994).

8. Rai, A. K., Rai, A., Ramaiya, A. J., Jha, R., Mallik, R. Molecular adaptations allow dynein to generate large collective forces inside cells. *Cell* **152**, 172-182 (2013).